第36卷第2期
2017年4月

红外与毫米波学报
J. Infrared Millim. Waves

Vol. 36, No. 2
April, 2017

文章编号: 1001-9014(2017)02-0160-07

DOI: 10.11972/j.issn.1001-9014.2017.02.007

Influence of microcavity effect on modulation response in 1.3 μm quantum dot photonic crystal nanocavity lasers

XING En-Bo[1,2], RONG Jia-Min[1,2], TONG Cun-Zhu[1*], TIAN Si-Cong[1], WANG Li-Jie[1], SHU Shi-Li[1], WANG Li-Jun[1]

(1. State Key Laboratory of Luminescence and Applications, Changchun Institute of Optics, Fine Mechanics and Physics, Chinese Academy of Sciences, Changchun 130033, China;
2. University of Chinese Academy of Sciences, Beijing 100049, China)

Abstract: It had been proposed that the microcavity effect could enhance the spontaneous emission rate and hence dramatically increase the modulation speed. However, the work in this paper reveals that the situation might not be completely correct for the 1.3 μm GaAs based quantum dot (QD) photonics crystal (PhC) nanolasers due to the complex carrier dynamics and close hole levels. Based on the all-pathway rate equation model considering the carrier relaxation dynamics, the influences of quality (Q) factor of cavity on the threshold and modulation responses of 1.3 μm QD PhC nanolasers were studied. It is found that the high Q factor can improve significantly the threshold of QD PhC nanolasers, but it also increases the photon lifetime and deteriorates the modulation bandwidth. Hence there exists an optimized Q factor (~2500) for the nanolaser with a modulation bandwidth exceeding 100 GHz. For the energy consumption, the best value corresponds to a Q factor of ~7 000. So an overall consideration is preferable in designing PhC nanocavity for both high speed and low energy consumption operation of QD lasers.

Key words: modulation response, photonics crystal laser, quantum dot, rate equation, threshold
PACS: 42.55.Tv, 78.67.Hc, 42.60.Fc

微腔效应对于1.3μm量子点光子晶体纳腔激光器调制响应的影响

邢恩博[1,2], 戎佳敏[1,2], 佟存柱[1*], 田思聪[1], 汪丽杰[1], 舒适立[1], 王立军[1]

(1. 中国科学院长春光学精密机械与物理研究所, 吉林 长春 130033;
2. 中国科学院大学, 北京 100049)

摘要: 微腔效应可以提高自发辐射速率, 从而起到有效的改善响应调制速率的作用. 然而, 对于1.3 μm GaAs/InAs量子点光子晶体激光器而言, 调制速率还会受到复杂的载流子动力学以及更近的空穴能级间隔的影响. 因此基于全路径载流子弛豫动力学方程, 计算并讨论了腔品质因子(Q)对于阈值和响应调制特性的影响. 计算结果表明, 高的Q值能够明显改善量子点光子晶体激光器的阈值, 但是同时快速增长的光子寿命会导致调制带宽的恶化. 所以, 存在一个优化的Q值(2500)可以获得超过100 GHz的调制带宽, 而当Q值为7 000时, 对应的能量传输损耗最低. 因此, 在量子点光子晶体纳腔激光器的设计中, 更全面的考虑各方面的因素对器件的性能的影响, 对于获得高速调制低功耗的量子点激光器器件是十分有意义的.

关 键 词: 调制响应; 光子晶体激光器; 量子点; 速率方程; 阈值

中图分类号: TN248.4 **文献标识码:** A

Introduction

Optical interconnects have attracted considerable interest owing to the lower power consumption compared with the traditional electrical connectivity in recent years.[1-5] Two-dimensional (2D) photonic-crystal (PhC) laser is recognized as one of these ideal candi-

Received date: 2016-07-05, **revised date:** 2016-12-13 **收稿日期:** 2016-07-05, **修回日期:** 2016-12-13
Foundation items: Supported by National Natural Science Foundation of China (61176046, 11304308), National Basic Research Program of China (2013CB933300)
Biography: HAO En-Bo (1986-), male, Jilin China, Ph. D. candidate. Research field is photonic crystal lasers. E-mail: xiaoxing1228@126.com
* **Corresponding author:** E-mail: tongcz@ciomp.ac.cn

dates because of its low threshold current [6], high speed modulation [7-8] and low power consumption. [9-10] Moreover, PhC laser might also be the most promising architecture for nanoscale integration. [11] Theoretical and experimental investigations have demonstrated that nanocavity can lead to much higher modulation speed than the edge-emitting or vertical-cavity surface-emitting lasers (VCSELs). [12-15] Exceeding 100 GHz modulation quantum well (QW) PhC lasers had been reported, [7] and a large-signal modulation of 30 GHz was achieved in quantum dot (QD) PhC lasers [16]. Compared with QW PhC lasers, the PhC nanolasers embedded QDs as gain material show lower threshold [6] due to the three-dimensional carrier confinement, low surface recombination rate and the discrete energy levels. Recently 1.3 μm InAs-GaAs QD lasers have made significant progresses [17], which lead to the potential possibility of 1.3 μm QD PhC nanocavity lasers for the high speed optical interconnects with long distance. [18-19] Intrinsically, the introducing of nanocavity in 1.3 μm InAs-GaAs QDs will also be helpful for overcoming the bandwidth limitation due to the close space of hole levels and broadening the realistic applications.

However, there is no clearly physical insight deep into the complex carrier dynamics in 1.3 μm InAs-GaAs QDs and the microcavity effect in the QD PhC nanocvity up to now. The results are also possible to be used in the inverse direction to the predication. For QD PhC nanocvity lasers, Purcell effect lowers the threshold through high spontaneous emission (SE) coupling factor (β), in the meantime, the modulation response is improved by enhancing the SE rate of QDs. High Purcell factor comes from the combination of small mode volume V_m and high quality factor (Q). However at the same time, the increase in the cavity photon lifetime t_p will limit the modulation response. The ultrahigh speed modulation response in nanocavity have been theoretically demonstrated based on rate equations [12, 20], but some important physical processes are ignored in these models due to the oversimplified rate equation model or the nanocavity effect without rigorous treatment. Therefore, it is significant to completely investigate carrier dynamics and modulation response in 1.3 μm QD PhC nanolaser. In addition, it is beneficial to design and fabricate PhC nanolasers with high speed low energy consumption in experiments, and is also meaningful to the development of microcavity lasers.

In this paper, a self-consistent all-pathway QD rate equation model [21] was used to analyze the carrier dynamics and modulation response of 1.3 μm InAs/GaAs QD PhC nanolasers, in which the influences of Q on SE rate, β factor, and the cavity photon lifetime were taken into account. The phonon-assisted relaxation, Auger-assisted relaxation, and the close spacing of holes levels features were directly introduced into calculations. The carrier occupation probabilities in QD energy levels and the threshold current density are shown at different Q, meanwhile, the influences of Q on the modulation response and energy consumption were also investigated.

1 Modeling

1.1 Carrier dynamics and all-pathway rate equation of 1.3 μm QD lasers

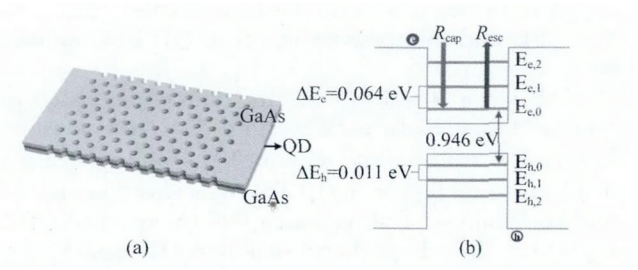

Fig. 1 Schematic diagram of (a) PhC nanocavity, and (b) all-pathway carrier relaxation in a 1.3 μm InAs/GaAs QD

图 1 (a) 光子晶体纳腔示意图,(b) 1.3 μm InAs/GaAs 量子点载流子全路径弛豫过程

As shown in Fig. 1 (a), one QD active layer is embedded in the middle of the membrane and an L3 nanocaivty formed by removing three holes in a line is introduced. The parameters used here include a lattice constant a of 350 nm and a slab thickness of 210 nm. The radius of the air hole is $0.3a$. In the 1.3 μm InAs/GaAs QD system, [22] there exists multi-levels for the holes, electrons, and also multiple possible relaxation pathways for carriers from the wetting layer (WL) to QD levels. The models based on the level-by-level relaxation are not applicable [23]. All-pathway QD rate equation model considers all the possible relaxation pathways and also the carrier transport dynamics in the barrier, it can reflect the realistic characteristics of 1.3 μm InAs/GaAs QD lasers [21]. Figure 1(b) shows that carriers injected into the barrier are able to relax to the ground state of QDs by releasing the energy to phonons or via the carrier-carrier scattering (Auger-assisted relaxation). The latter is proportional to the two dimensional carrier density and plays an important role at high injected current. Hence, the relaxation rates can be written as:

$$R_{ij}(i \neq j) = A_{ij} + C_{ij}N_w \quad , \quad (1)$$

where subscripts $i, j = 0, 1, 2, w$ represent the ground state, the first excited state, the second excited state, and the lowest energy level in WL or cap layer (CL), respectively. A_{ij} is the phonon-assisted relaxation rate and C_{ij} is Auger-assisted relaxation coefficient from i_{th} to j_{th}. N_w is the carrier density in the WL or CL. Correspondingly, the carrier escape rates in the intra-band can be expressed as follows when the WL energy band is below the quasi-Fermi level [21],

$$Es_{ij}(i < j) = \frac{P_j}{P_i}\exp\left(-\frac{E_{ij}}{k_BT}\right)R_{ij} \quad , \quad (2)$$

and from QD levels to the WL (CL) is

$$Es_{iw} = \frac{g_w}{2p_i\rho}\exp\left(-\frac{E_{iw}}{k_BT}\right)R_{wi} \quad , \quad (3)$$

where p_i is the degeneracy of QD levels, ρ is the surface density of QDs. E_{ij} is the energy separation between different QD levels and E_{iw} is the energy separation between WL and every energy levels in QDs. k_B and T correspond to the Boltzmann's constant and temperature. g_w describes the carrier concentration in the WL(CL). The carrier relaxation dynamics in 1.3 μm InAs/GaAs QDs can be described in above three equations. The detailed rate equations are listed in Appendix A, and more de-

scription on this model can be found in Ref. 21.

1.2 SE and microcavity effect in QD PhC nanocavity

SE factor β is defined as the ratio of the SE coupled into the lasing mode over the total SE. In conventional lasers, β is typically the order of 10^{-6}, while β can reach 0.22 and even higher in QD PhC nanocavity lasers. [5,24] The contribution of SE coupling into cavity should not be neglected. Based on the all-pathway QD model, an equation describing the photon number is modified as below:

$$\frac{dS}{dt} = \frac{v_g g_{max}(f_{0e}+f_{0h})S}{1+S\Gamma\varepsilon_m/V_D} - \frac{S}{t_p} + \frac{\beta\rho S_a p_0(f_{0e}+f_{0h})}{t_{r0}} \quad (4)$$

where v_g, t_{r0}, t_p, S_a and V_D are the group velocity, SE lifetime, photon lifetime, the area of active region and the volume of all QDs in the active region, respectively. Surface density of QDs ρ is selected as 3×10^{10} cm^{-2} in this simulation. It means about several hundred QDs in the nanocavity. f_{0e} and f_{0h} are electron and hole occupation probability, respectively, at the ground state. The maximum modal gain g_{max} is described using the equation in Ref. 25. The third term on the right of Eq. 4 represents the number of SE coupled into the cavity mode. ε_m is the nonlinear gain coefficient, [26] and the optical confinement factor Γ is selected as 0.01 according to the experimental results. [24] The corresponding definitions and values of above parameters are listed in Table 1.

For a single QD emitter, β can be approximately expressed as $\beta\approx1-(t_{r0}/t_2)$, [26] where t_2 is the lifetime for off-resonant QD, which is longer than the intrinsic value due to the photonic band gap effect. The value of $\beta\sim0.97$ can be reached for single QD at low temperature. [26] However, in the multi-QD system, the spectral width of the cavity mode is much smaller than the inhomogeneous broadening of QDs. It means that the lasing mode is supported by the QDs only, spatially in the cavity and spectrally overlap. Hence a factor is required to amend β, which is approximately expressed as the ratio of inhomogeneous broadening of single QD and multi-QDs. In our simulation, the inhomogeneous broadening of the ground state at 300 K is ~35 meV for multi-QDs and ~10 meV [27] for single QD. t_2 is selected as 3 ns. Hence the SE coupling factor β can be modified as $\beta\approx0.29[1-(t_{r0}/t_2)]$. The calculated value of β is in the range of 0.2~0.29, which is in agreement with the experiment results. [5,24]

The SE lifetime (t_{r0}) is shortened in nanocavity and can be expressed as: [28]

$$\frac{t_0}{t_{r0}} = F_{cav}\left(\frac{\boldsymbol{E}(\boldsymbol{r}_A)\boldsymbol{\mu}}{|\boldsymbol{E}_{max}||\boldsymbol{\mu}|}\right)^2 \frac{1}{1+4Q^2\left(\frac{\lambda}{\lambda_{cav}}-1\right)^2} + F_{PhC} \quad (5)$$

where t_0 is the SE lifetime in bulk material. λ_{cav} is the wavelength of cavity mode. $\left(\frac{\boldsymbol{E}(\boldsymbol{r}_A)\boldsymbol{\mu}}{|\boldsymbol{E}_{max}||\boldsymbol{\mu}|}\right)^2$ and $\frac{1}{1+4Q^2\left(\frac{\lambda}{\lambda_{cav}}-1\right)^2}$ represent the spatial and spectral mismatch between the emitter dipole and the cavity, respectively. The second term F_{PhC} describes a decay channel due to SE coupling into quasi-photonic band gap. [29] F_{cav} is the Purcell factor and can be written as

$$F_{cav} = \frac{3}{4\pi^2}\frac{\lambda_{cav}^3}{n_{eff}^3}\frac{Q}{V_m} \quad (6)$$

where V_m is the cavity-mode volume and n_{eff} is the refractive index of materials in nanocavity.

1.3 Small-signal analysis

Based on the all-pathway rate equations, the small-signal current injection with modulation angular frequency of ω is $J=J_0+\Delta J\exp(j\omega t)$. The corresponding signal response is $S=S_0+\Delta S\exp(j\omega t)$. Here S_0 is the photon number in the cavity at steady state with J_0. ΔJ is the modulation amplitude. Subsequently, the carriers in barrier can be described as Eq. (7). Equations (8-11) represent the carrier occupation probabilities in WL (or CL), the ground state, first exited state, and second excited state in the QDs, respectively.

$$N_B = N_{B0} + \Delta N_B\exp(j\omega t) \quad (7)$$
$$f_W = f_{W0} + \Delta f_W\exp(j\omega t) \quad (8)$$
$$f_0 = f_{00} + \Delta f_0\exp(j\omega t) \quad (9)$$
$$f_1 = f_{10} + \Delta f_1\exp(j\omega t) \quad (10)$$
$$f_2 = f_{20} + \Delta f_2\exp(j\omega t) \quad (11)$$

Equations. (7-11) are substituted into Eqs. (A1-A5) shown in Appendix A to obtain the modulation response function, which is described as Eq. (12). Here the subscripts e and h represent electron and hole, respectively. The other corresponding parameters are shown in Appendix B.

$$M(\omega) = q\frac{|\Delta S|}{|\Delta J|} = \frac{\left|\frac{X_e}{F_e}+\frac{X_h}{F_h}\right|\left|\frac{v_g g_{max}S_0}{1+\varepsilon S_0}+\frac{\beta p_1\rho S_a}{t_{r0}}\right|}{\left|j\omega-\frac{v_g g_{max}(f_{e0}+f_{h0}-1)}{1+\varepsilon S_0}+\frac{1}{t_p}+\frac{v_g g_{max}(f_{e0}+f_{h0}-1)}{2p_0\rho S_a(1+\varepsilon S_0)}\left(\frac{Y_e}{F_e}+\frac{Y_h}{F_h}\right)\right|} \quad (12)$$

2 Results and discussion

The enhanced Q factor in PhC nanocavity will affect the carrier dynamics and hence the modulation performance, one of the important influences is on the carrier occupation probabilities of QD levels, which are calculated and shown in Fig. 2 for electrons f_{0e} (solid symbols) and holes f_{0h} (hollow symbols) as functions of injected current density at 300 K. Here Q factors are selected as 2000 (squares), 5000 (circles) and 10000 (upper triangles), respectively. It can be seen that f_{0e} shows much higher occupation probabilities than f_{0h} at the same current density, which can be attributed to the close energy spacing of the hole levels. [30] The increase in Q factor in nanocavity results in the decrease in occupation probabilities of QDs, since a high Q corresponds to a high SE rate and thus a short time of the carrier staying at ground state. For high injected current density, the effect of Q factor on electrons is relatively smaller than that of holes, meaning that the modulation of Q factor on carrier dynamics is determined more by holes under the condition of high injected current.

The influence of Q on the threshold current density

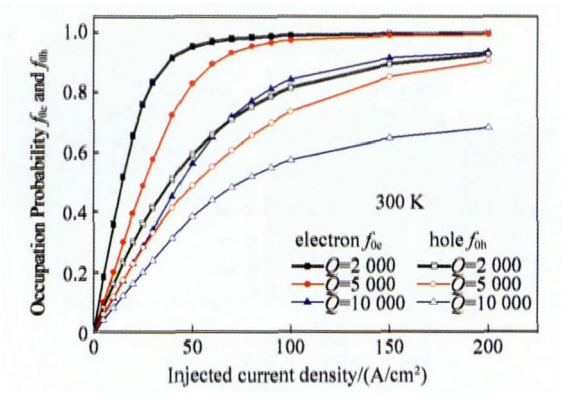

Fig. 2　Occupation probabilities for electrons f_{0e} (solid symbols) and holes f_{0h} (hollow symbols) as functions of injected current density at 300 K for different Q

图 2　温度为 300 K 时,电子(实心符号)和空穴(空心符号)的占据几率随着 Q 值的变化

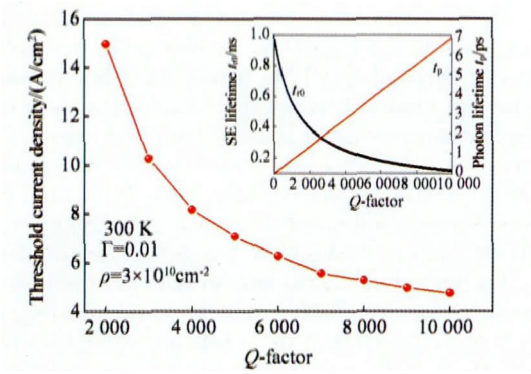

Fig. 3　The influence of Q on the threshold current density J_{th} at 300 K. The inset shows t_{r0} and t_p as functions of Q factor

图 3　在 300 K 时,Q 值对于阈值电流密度的影响. 插图为 Q 值对于 t_{r0} 和 t_p 的影响

(J_{th}) at 300 K is shown in Fig. 3 with Q value from 2000 to 10000. In the calculation, the threshold condition is defined as the cavity photon number $S=1$ by solving Eq. (4) [12]. It can be seen that J_{th} reduces gradually with the increase of Q, and then tends to vary gently. The minimum J_{th} of 4.8 A/cm^2 can be obtained for the Q value of 10000, which is only about one-third of that under the condition of $Q\sim2000$. In the nanocavity with high Purcell factor, the threshold is reduced through suppression of SE into non-lasing modes, [28] meanwhile higher SE factor means shorter SE lifetime. The other contribution to the improvement of threshold is the low cavity leakage-rate of photon, which is inversely proportional to the photon lifetime and is able to be expressed as $1/t_p$. To understand the mechanism behind, the calculated SE lifetime at ground state t_{r0} and photon lifetime t_p are plotted in the inset of Fig. 3. t_p shows a linear dependence on the Q factor, while SE lifetime t_{r0} decreases with the increase of Q factor, which is similar to the trend of threshold affected by Q factor.

To disclose the influence of injected current density (J) on the modulation characteristics of 1.3 μm InAs/GaAs QD nanocavity lasers, the modulation response as function of J for $Q\sim2000$ and $Q\sim7000$ at 300 K were calculated and shown in Fig. 4. The selection of relaxation parameters in calculation was according to the experimental and theoretical results in a real QD system. [31] Only the intrinsic modulation response was considered. The effect from the resistance and capacity of devices is not the main topic of this work. It shows that the nonzero resonance frequencies increase and the resonances quench with the increase in injected current. It is attributed to the increase in damping factor which increases in proportion to resonance frequency under high injected current level. The nanocavity laser with $Q\sim2000$ reveals a higher bandwidth than that of $Q\sim7000$, and the maximum modulation bandwidth of $Q\sim2000$ exceeds 100 GHz from Fig. 4(a). This dependence is also in agreement with the analysis in Ref. 8. The behind mechanism can be attributed to the dramatic decrease in SE lifetime and increase in photon lifetime, which determine the bandwidth. High Q can reduce SE lifetime and thus lead to high modulation bandwidth, but as Q continues to increase, the increase in photon lifetime will restrict the modulation bandwidth. The opposite dependences of SE lifetime and photon lifetime on Q factor have been shown in the inset of Fig. 3. Therefore, a high Q cavity has a reduced modulation bandwidth, which is mainly limited by photon lifetime and the saturation of SE rate. In addition, the modulation bandwidth for high Q factor is much higher than that of the macroscopic 1.3 μm InAs-GaAs QD edge-emitting lasers. [11, 32] This might originates from

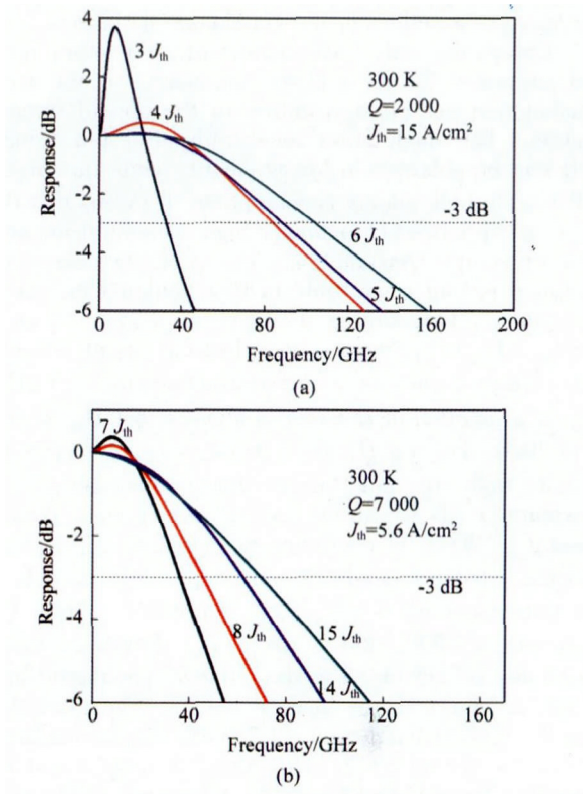

Fig. 4　Calculated modulation response of 1.3 μm QD lasers for different injected current density with $Q=2000$ and $Q=7000$

图 4　Q 值分别为 2000 和 7000 时,1.3 μm 量子点激光器的响应调制与注入电流密度的关系

the microcavity effect in the simulated QD lasers.

Comparing with 3 dB bandwidth, the other important parameter for the realistic application is the energy consumption per bit transmitted in the optical interconnection. The modulation bandwidth of a few hundred GHz can be obtained in low Q cavity, while the large J_{th} will lead to high energy consumption. It means that there exists an optimized Q factor for high speed and low interconnect energy consumption. The accurate energy consumption per bit is not able to be calculated due to that the voltage information is absent in our model. So we use 3 dB_{max}/J_{max} to approximately reflect the energy consumption. Figure 5 shows that the maximum value of 3 dB_{max}/J_{max} as a function of Q factor is about 2.6 GHz/Acm^{-2} at Q of 7000. For low Q value, 3 dB_{max}/J_{max} is mainly limited by high injected current density because that the maximum 3 dB bandwidth is realized at more than ten times J_{th}. When Q continues to increase, J_{th} decreases and the maximum bandwidth occurs at a few times J_{th}, so the corresponding 3 dB_{max}/J_{max} increases. When Q is higher than 7000, the 3 dB_{max}/J_{max} decreases slowly, which can be attributed to the reduced modulation bandwidth, as shown in the inset of Fig. 5. The inset shows that the highest bandwidth ~120 GHz can be realized at a Q factor around 2500. After that, it reduces and is about 66 GHz at Q factor ~7000. Of course, these values in the realistic devices will be also dependent on the detailed device characteristics, such as QD density, inhomogeneous broadening, series resistance, and capacitance, etc.

Table 1 Parameters used in the rate equations
表1 在速率方程中使用的参数

Symbol	Meaning	Value
t_{ri} (i = B, w, 1, 2)	SE lifetime in the barrier, WL, the first excited state and the second excited state of QDs, respectively.	1 ns
t_{bw}	Carrier transport time from cladding layer to the nearest WL(CL).	Ref. [21]
t_{ewb}	Carrier escape time from WL(CL) to the GaAs barrier.	1.12 ps(electron) 0.35 ps(hole) at 300 K
b	the thickness of the GaAs barrier	10 nm
f_i (i = B, w, 1, 2)	Carrier occupation probability in the barrier, WL, the first excited state and second excited state of QDs, respectively	
g_w	Parameter describing the carrier concentration in the WL(CL)	5.13×10^{15} m^{-2}(electron) 3.56×10^{16} m^{-2}(hole)
v_g	Group velocity	8.8×10^{7} m/s
ρ	QD density	3×10^{10} cm^{-2}
q	Electronic charge	1.6×10^{-19} C
h	Planck's constant	6.626×10^{-34} Js
m_0	Rest mass of electron	9.1×10^{-31} Kg
ε_0	Absolute permittivity in vacuum	8.854×10^{-12} F/m
k_B	Boltzmann's constant	1.38×10^{-23} J/K

3 Conclusion

In summary, we have investigated the modulation responses of 1.3 μm InAs/GaAs QD PhC nanolasers using self-consistent all-pathway QD rate equation model. It is shown that the high Q factor can improve significantly the threshold of QD PhC nanolasers, but it will also increase the photon lifetime and deteriorate the modulation performance. Although SE lifetime is improved with the increase in Q factor and hence benefit for bandwidth, this effect tends to saturate for high Q factor. Hence there exists an optimized Q factor (~2500) for the nanolaser with a modulation bandwidth exceeding 100 GHz. For the energy consumption per bit, the best value occurs at Q factor ~7000, and the corresponding bandwidth is about 66 GHz. Our results are benefit for the development of high speed low energy consumption QD nanocavity lasers.

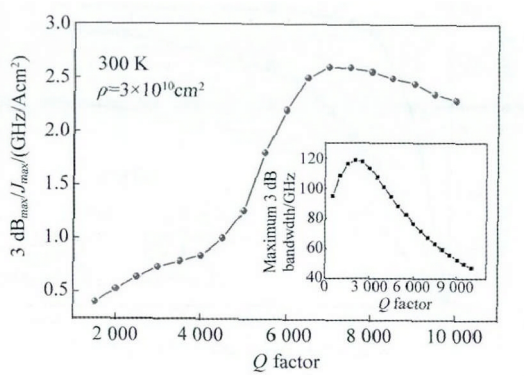

Fig. 5 3 dB_{max}/J (GHz/A cm^{-2}) as a function of Q at 300 K, the inset shows 3 dB_{max} at different Q factor

图5 温度为300 K时,3 dB_{max}/J (GHz/A cm^{-2})随Q值的变化,插图为3 dB_{max}随Q值的变化关系

Acknowledgments

This work was supported by National Natural Science Foundation of China (No. 61176046, No. 11304308), and National Basic Research Program of China (2013CB933300).

Appendix A: Rate equations

$$\frac{dN_B}{dt} = \frac{J}{qb} + \frac{g_w f_w}{t_{ewb} b}(1 - f_B) - \left(\frac{1}{t_{bw}} + \frac{1}{t_{rB}}\right) N_B \quad ,(A1)$$

$$\frac{df_w}{dt} = \sum_{i=0}^{2}\left[\frac{2p_i\rho}{g_w} E_{siw} f_i(1 - f_w) - R_{wi} f_w(1 - f_w)\right] + \frac{(1 - f_w) N_B}{g_w t_{bw}} - \frac{f_w}{t_{ewb}} - \frac{f_w}{t_{rw}} \quad ,(A2)$$

$$\frac{df_2}{dt} = \left[\frac{g_w}{2p_2\rho} R_{w2} f_w(1 - f_2) - E_{s2w}(1 - f_w)\right] + \sum_{i}^{1}\left[\frac{p_i}{p_2} E_{si2} f_i(1 - f_2) - R_{2i} f_2(1 - f_i)\right] - \frac{f_2}{t_{r2}} \quad ,(A3)$$

$$\frac{df_1}{dt} = \left[\frac{g_w}{2p_1\rho} R_{w1} f_w(1 - f_1) - E_{s1w} f_1(1 - f_w)\right] + \left[\frac{p_2}{p_1} R_{21} f_2(1 - f_1) - E_{s12} f_1(1 - f_2)\right]$$

$$+\left[\frac{p_0}{p_1}E_{s01}f_0(1-f_1)-R_{10}f_1(1-f_0)\right]-\frac{f_1}{t_1} \quad ,(A4)$$

$$\frac{\mathrm{d}f_0}{\mathrm{d}t}=\left[\frac{g_w}{2p_0\rho}R_{w0}f_w(1-f_0)-E_{s0w}f_0(1-f_w)\right]+\sum_i^2\left[\frac{p_i}{p_0}R_{i0}f_i(1-f_0)-E_{s0i}f_0(1-f_i)\right]-\frac{f_1}{t_1}-\frac{1}{2p_0\rho S_a}\frac{v_g g_{\max}(f_{0e}+f_{0h}-1)S}{1+\varepsilon S} \quad .(A5)$$

Appendix B: Parameters for small-signal modulation

$$A_1=j\omega+\frac{1-f_{w0}}{t_{bw}}+\frac{1}{t_{rB}}$$

$$B_1=\frac{g_w}{b}\frac{1}{t_{ewb}}-\frac{N_{B0}}{t_{bw}}$$

$$A_2=-\frac{b}{g_w t_{bw}}$$

$$B_2=j\omega+\frac{2p_0\rho}{g_w}E_{s0w}f_{00}+\frac{2p_1\rho}{g_w}E_{s1w}f_{10}+\frac{2p_2\rho}{g_w}E_{s2w}f_{20}+R_{w0}(1-f_{00})+R_{w1}(1-f_{10})+R_{w2}(1-f_{20})+\frac{1}{t_{ewb}}+\frac{1}{t_{rw}}$$

$$C_2=-\frac{2p_2\rho E_{s2w}}{g_w}(1-f_{00})-R_{w2}f_{w0}$$

$$D_2=-\frac{2p_1\rho E_{s1w}}{g_w}(1-f_{w0})-R_{w1}f_{w0}$$

$$E_2=-\frac{2p_0\rho E_{s0w}}{g_w}(1-f_{w0})-R_{w0}f_{w0}$$

$$B_3=-\frac{g_w}{2p_2\rho}R_{w2}(1-f_{20})-E_{s2w}f_{20}$$

$$C_3=j\omega+\frac{g_w}{2p_2\rho}R_{w2}f_{w0}+E_{s2w}(1-f_{w0})+\frac{p_0}{p_2}E_{s0w}f_{00}+R_{20}(1-f_{00})+\frac{p_1}{p_1}E_{s12}f_{10}+R_{21}(1-f_{10})+\frac{1}{t_{r2}}$$

$$D_3=-\frac{p_1}{p_2}E_{s12}(1-f_{20})-R_{21}f_{20}$$

$$D_3=-\frac{p_0}{p_2}E_{s02}(1-f_{20})-R_{20}f_{20}$$

$$B_4=-\frac{g_w}{2p_1\rho}R_{w1}(1-f_{10})-E_{s1w}f_{10}$$

$$C_4=-\frac{p_2}{p_1}R_{21}(1-f_{10})-E_{s12}f_{10}$$

$$D_4=j\omega+\frac{g_w}{2p_1\rho}R_{w1}f_{w0}+E_{s1w}(1-f_{w0})+\frac{p_2}{p_1}R_{21}f_{20}+E_{s12}(1-f_{20})+\frac{p_0}{p_0}E_{s01}f_{00}+R_{10}(1-f_{00})+\frac{1}{t_{r1}}$$

$$E_4=-\frac{p_0}{p_1}E_{s01}(1-f_{10})-R_{10}f_{10}$$

$$B_5=-\frac{g_w}{2p_0\rho}R_{w0}(1-f_{00})-E_{s2w}f_{00}$$

$$C_5=-\frac{p_2}{p_0}R_{20}(1-f_{00})-E_{s2w}f_{00}$$

$$E_5=j\omega+\frac{g_w}{2p_0\rho}R_{w0}f_{w0}+E_{s0w}(1-f_{w0})+\frac{p_1}{p_0}R_{10}f_{10}+E_{s1w}(1-f_{10})+\frac{p_2}{p_0}R_{20}f_{20}+E_{s2w}(1-f_{20})+\frac{1}{t_{r0}}+\frac{v_g g_{\max}}{p_0\rho S}\frac{S_0}{1+\varepsilon S_0}$$

$$Y=\begin{vmatrix}A_1 & B_1 & 0 & 0\\ A_2 & B_2 & C_2 & D_2\\ 0 & B_3 & C_3 & D_3\\ 0 & B_4 & C_4 & D_4\end{vmatrix} \quad X=\begin{vmatrix}A_2 & B_2 & C_2 & D_2\\ 0 & B_3 & C_3 & D_3\\ 0 & B_4 & C_4 & D_4\\ 0 & B_5 & C_5 & D_5\end{vmatrix}$$

$$F=\begin{vmatrix}A_1 & B_1 & 0 & 0 & 0\\ A_2 & B_2 & C_2 & D_2 & E_2\\ 0 & B_3 & C_3 & D_3 & E_3\\ 0 & B_4 & C_4 & D_4 & E_4\\ 0 & B_5 & C_5 & D_5 & E_5\end{vmatrix}$$

References

[1] Almeida V R, Barrios C A, Panepucci R R, *et. al*. All-optical control of light on a silicon chip [J]. *Nature*, 2004, **431**: 1081-1084.

[2] David A, Miller B. Device requirements for optical interconnects to silicon chips [J]. *Proc. IEEE*, 2009, **97**(7): 1166-1185.

[3] Zhang Z C, You Z, Chu D P. Fundamentals of phase-only liquid crystal on silicon (LCOS) devices Open [J]. *Light-Sci. Appl*. 2014, **3**: e213.

[4] Gu M, Li X P, Cao Y Y. Optical storage arrays: a perspective for future big data storage Open [J]. *Light-Sci. Appl*., 2014, **3**: e177.

[5] Strauf S, Jahnke F. Single quantum dot nanolaser [J]. *Laser Photon. Rev*., 2011, **5**(5): 607-633.

[6] Ellis B, Mayer M A, Shambat G, *et al*. Ultralow-threshold electrically pumped quantum dot photonic-crystal nanocavity laser [J]. *Nat. Photon*, 2011, **5**(5): 297-300.

[7] Altug H, Englund D, VuCkovi J. Ultrafast photonic crystal nanocavity laser [J]. *Nat. Physics*, 2006, **2**(2): 484-488.

[8] Englund D, Altug H, Ellis B, *et al*. Ultrafast photonic crystal lasers [J]. *Laser Photon. Rev*., 2008, **2**(4): 264-274.

[9] Matsuo S, Shinya A, Chen C H, *et al*. 20-Gbit/s directly modulated photonic crystal nanocavity laser with ultra-low power consumption [J]. *Opt. Express*, 2011, **19**(3): 2242-2250.

[10] Takeda K, Sato T, Shinya A, *et al*. Few-fJ/bit data transmissions using directly modulated lambda-scale embedded active region photonic-crystal lasers [J]. *Nat. Photon*, 2013, **7**(7): 569-575.

[11] Chen C H, Takeda K, Shinya A, *et al*. 40-Gb/s directly-modulated photonic crystal lasers under optical injection-locking [J]. *Opt. Express*, 2011, **19**(18): 17669.

[12] Bjork G, Yamamoto Y. Analysis of semiconductor microcavity lasers using rate equations [J]. *IEEE J. Quantum Electron*, 1999, **23**(11): 2386-2396.

[13] Lorke M, Nielsen T R, M? rk J. Influence of carrier dynamics on the modulation bandwidth of quantum-dot based nanocavity devices [J]. *Appl. Phys. Lett*., 2010, **97**(21): 211106-211106-3.

[14] Tong C Z, Xu D, Soon F Y. Carrier relaxation and modulation response of 1.3 μm InAs-GaAs quantum dot lasers [J]. *J. Lightwave Technol*., 2009, **27**(23): 5442-5450.

[15] Xiao J L, Huang Y Z. Numerical analysis of gain saturation, noise figure, and carrier distribution for quantum-dot semiconductor-optical amplifiers [J]. *IEEE J. Quantum Electronics*, 2008, **44**(5): 448-455.

[16] Ellis B, Fushman I, Englund D, *et al*. Dynamics of quantum dot photonic crystal lasers [J]. *Appl. Phys. Lett*., 2007, **90**(15): 151102.

[17] Zeghuzi1 A, Schmeckebier H, Stubenrauch M, *et al*. 25 Gbit/s differential phase-shift-keying signal generation using directly modulated quantum-dot semiconductor optical amplifiers [J]. *Appl. Phys. Lett.*, 2010, **106**(21): 213501.
[18] Meuer C, Kim J, Laemmlin M, *et al*. 40 GHz small-signal cross-gain modulation in 1.3 m quantum dot semiconductor optical amplifiers [J]. *Appl. Phys. Lett.*, 2008, **93**: 051110.
[19] Kim S M, Wang Y, Keever M, et al. High-frequency modulation characteristics of 1.3 μm InGaAs quantum dot lasers [J]. *IEEE Photon. Technol. Lett.*, 2004, **16**(2): 377-379.
[20] Shore K A. Modulation bandwidth of metal-clad semiconductor nanolasers with cavity-enhanced spontaneous emission [J]. *Electron. Lett.*, 2010, **46**(25): 1688-1689.
[21] Tong C Z, Yoon S F, Ngo C Y, *et al*. Rate equations for 1.3 μm dots-under-a-well and dots-in-a-well self-assembled InAs - GaAs quantum-dot Lasers [J]. *IEEE J. Quantum Electron*, 2006, **42**(11): 1175-1183.
[22] Borri P, Langbein W, Hvam J M, *et al*. Spectral hole-burning and carrier-heating dynamics in InGaAs quantum-dot amplifiers [J]. *IEEE J. Sel. Top. Quantum Electron*, 2000, **6**(3): 544-551.
[23] Fiore A, Borri P, Langbein W, *et al*. Time-resolved optical characterization of InAs/InGaAs quantum dots emitting at 1.3 μm [J]. *Appl. Phys. Lett.*, 2000, **76**(23): 3430-3432.
[24] Nomura M, Iwamoto S, Watanabe M, *et al*. Room temperature continuous-wave lasing in photonic crystal nanocavity [J]. *Opt. Express*, 2006, **14**(13): 6308-6315.
[25] Sugawara M. *Semiconductor and semimetals* [M]. New York: Academic, 1999.
[26] Chang W H, Chen W Y, Chang H S, *et al*. Efficient single-photon sources based on low-density quantum dots in photonic-crystal nanocavities [J]. *Phys. Rev. Lett.*, 2006, **96**(11): 117401-1-4.
[27] Bayer M. Forchel A. Temperature dependence of the exciton homogeneous linewidth in $In_{0.60}Ga_{0.40}As$/GaAs self-assembled quantum dots [J]. *Phys. Rev. B.*, 2002, **65**(4): 321-325.
[28] Englund D, Fattal D. Waks E, *et al*. Controlling the spontaneous emission rate of single quantum dots in a two-dimensional photonic crystal [J]. *Phys. Rev. Lett.*, 2005, 95(1): 013904-1-4.
[29] Kress A, Hofbauer F, Reinelt N, *et al*. Manipulation of the spontaneous emission dynamics of quantum dots in two-dimensional photonic crystals [J]. *Phys. Rev. B.*, 2005, 200571(24): 241304-1-4.
[30] Park G, Shchekin O B, Deppe D G. Temperature dependence of gain saturation in multilevel quantum dot lasers [J]. *IEEE J. Quantum Electron*, 2000, **36**(9): 1065-1071.
[31] Nielsen T R, Gartner P, Jahnke F. Many-body theory of carrier capture and relaxation in semiconductor quantum-dot lasers [J]. *Phys. Rev. B.*, 2004, **69**(23): 517-519.
[32] Tong C Z, Xu D W, Yoon S F. Carrier relaxation and modulation response of 1.3 μm InAs - GaAs quantum dot lasers [J]. *J Lightwave Technol.*, 2009, **27**(23): 5442-5450.